University of Huddersfield Repository

Van den Berg, Jakob, Reading, M.A., Bailey, P., Noakes, T.Q.C., Adelmann, C., Popovici, M., Tielens, H., Conard, T., de Gendt, S. and van Elshocht, S.

Medium energy ion scattering for the high depth resolution characterisation of high-k dielectric layers of nanometer thickness

Original Citation

Van den Berg, Jakob, Reading, M.A., Bailey, P., Noakes, T.Q.C., Adelmann, C., Popovici, M., Tielens, H., Conard, T., de Gendt, S. and van Elshocht, S. (2013) Medium energy ion scattering for the high depth resolution characterisation of high-k dielectric layers of nanometer thickness. Applied Surface Science. ISSN 0169-4332 (In Press)

This version is available at http://eprints.hud.ac.uk/16874/

The University Repository is a digital collection of the research output of the University, available on Open Access. Copyright and Moral Rights for the items on this site are retained by the individual author and/or other copyright owners. Users may access full items free of charge; copies of full text items generally can be reproduced, displayed or performed and given to third parties in any format or medium for personal research or study, educational or not-for-profit purposes without prior permission or charge, provided:

- The authors, title and full bibliographic details is credited in any copy;
- A hyperlink and/or URL is included for the original metadata page; and
- The content is not changed in any way.

For more information, including our policy and submission procedure, please contact the Repository Team at: E.mailbox@hud.ac.uk.

http://eprints.hud.ac.uk/

Medium Energy Ion Scattering for the high depth resolution characterization of high-*k* dielectric layers of nanometer thickness.

J. A. van den Berg *[a, b], M. A. Reading [b], P. Bailey [a], T. Q. C. Noakes [c], C. Adelmann[d], M. Popovici[d], H. Tielens[d], T. Conard[d], S. de Gendt[d,e] and S. van Elshocht[d] .

[a] *International Institute for Accelerator Applications, University of Huddersfield, Queensgate Huddersfield, HD1 3DH UK*

[b] *Physics and Materials Research Centre, University of Salford, Salford, M5 4WT, UK*

[c] *STFC Daresbury Laboratory, Daresbury, WA4 4AD, UK*

[d] *Imec, 75 Kapeldreef, 3001 Leuven, Belgium*

[e] *Also at Katholieke Universiteit Leuven, Celestijnenlaan 200F, B-3001 Leuven, Belgium*

Abstract

Medium energy ion scattering (MEIS) using, typically, 100 - 200 keV H^+ or He^+ ions derives it ability to characterize nanolayers from the fact that the energy after backscattering depends i) on the elastic energy loss suffered in a single collision with a target atom and ii) on the inelastic energy losses on its incoming and outgoing trajectories. From the former the mass of the atom can be determined and from the latter its depth. Thus MEIS yields depth dependent compositional and structural information, with high depth resolution (sub-nm near the surface) and good sensitivity for all but the lighter masses. It is particularly well suited for the depth analysis of high-k multilayers of nanometer thickness. Accurate quantification of the depth distributions of atomic species can be obtained using suitable spectrum simulation.

In the present paper, important aspects of MEIS including quantification, depth resolution and spectrum simulation are briefly discussed. The capabilities of the technique in terms of the high depth resolution layer compositional and structural information it yields, is illustrated with reference to the detailed characterization of a range of high–k nanolayer and multilayer structures for current microelectronic devices or those still under development: i) HfO_2 and HfSiOx for gate dielectric applications, including a TiN/ Al_2O_3/ HfO_2/ SiO_2 / Si structure, ii) TiN/ $SrTiO_3$/ TiN and iii) TiO_2/ Ru/ TiN multilayers structures for metal-insulator-metal capacitors (MIMcaps) in DRAM applications.

The unique information provided by the technique is highlighted by its clear capability to accurately quantify the composition profiles and thickness of nanolayers and complex multilayers as grown, and to identify the nature and extent of atom redistribution (e.g. intermixing, segregation) during layer deposition, annealing and plasma processing. The ability makes it a valuable tool in the development of the nanostructures that will become increasingly important as device dimensions continue to be scaled down.

Keywords

Medium energy ion scattering analysis, High resolution depth profiling, High-*k* nanolayers, Metal-insulator-metal capacitor (MIMcap) layers

1. Introduction

The ongoing scale reduction in microelectronic devices over the last decade or so has been enabled by a number of factors, including advanced processing technologies and novel materials development. Within the latter category a vitally important one has been the development of new dielectric materials having a dielectric constant substantially higher that SiO_2 (k = 3.9) for which the tunneling leakage currents at oxide thicknesses below ~1.5 nm were becoming unacceptable. Of the many metal oxides investigated [1, 2], Hf based dielectrics became the most promising high-*k* materials. Hafnia (HfO_2) has a medium high-*k* value (~20) and has good thermodynamic stability against Si [3] among other factors. The use of hafniumsilicate (HfSiOx) yields an improved re-crystallization temperature and leakage current but results in a somewhat reduced *k* value [4]. Due to their higher *k* values compared to SiO_2 these materials enable equivalent oxide thicknesses (EOT) down to ~1 nm. HfO_2 gate dielectrics in combination with a sub nanometer SiO_2 and metal gate (HKMG) were introduced in complementary metal-oxide semiconductor (CMOS) microprocessor device production in 2007.

Beyond gate oxide applications there is also a considerable interest in the application of high-*k* dielectric materials for mass storage devices e.g. high capacitance metal-insulator-metal capacitors (MIMcaps) for dynamic random access memory (DRAM) applications. These devices require EOT values of ≤ 0.4 nm in combination with very low leakage current densities, i.e. less than 10^{-7} A/cm^2 [5, 6] and, as for gate oxides, developments are driven by down scaling. Of the considerable range of materials and growth methods of these layers for memory applications investigated in recent years, $Sr_xTi_{1-x}O_3$ (STO) nanolayers either Sr enriched or stoichiometric ($k \geq 200$), in combination with TiN electrodes [5, 7] as well as TiO_2 ($k \geq 80$), as an attractive alternative to STO, and combined with Ru/RuO_2 electrodes [8, 9] have emerged as suitable, very high–k materials and have become the subject of intensive investigation and development. Considerable progress in the growth by atomic layer deposition (ALD) of such layers either in planar or trench structures has been made in recent years [7, 9, 10]. During processing such structures are routinely exposed to high temperatures. As not all layer combinations are thermally stable interdiffusion and interface reactions may occur. Thus the performance of the device will depend on its post anneal structure, composition depth profiles and layer thicknesses among others and an understanding of the operation of the device is contingent on the ability to characterize the physical structure, composition depth profiles and interface effects.

Comparatively few analytical techniques are capable of providing this range of information, with angular resolved ARXPS and high resolution (HR)RBS being some of them [11]. Medium energy ion scattering (MEIS) with its compositional and structural characterization capability at sub-nm depth resolution near the surface represent another option..

In this work we report on the high depth resolution application of MEIS to the characterization of a range of layers and multilayers of nanometer thickness for

current devices or those being developed: i) HfO_2 and HfSiOx, including a TiN/ Al_2O_3/ HfO_2/ SiO_2 /Si structure, ii) TiN/ $SrTiO_3$/ TiN and iii) TiO_2/ Ru/ TiN multilayers for metal-insulator-metal capacitor (MIMcap) structures in DRAM applications. MEIS is shown to provide unique information on elemental depth profiles, layer thickness, interdiffusion and segregation at interfaces and other effects due to processing and layer deposition. Preceding this, MEIS analysis will be briefly described and important aspects such as depth resolution, quantification and spectrum simulation discussed.

2. MEIS analysis

MEIS depth profiling is based on the energy analysis of energetic He or H ions, typically between 100-200 keV, backscattered from the nanolayer(s) through a fixed angle. It can be viewed as a low energy enhancement of Rutherford backscattering/ channeling, capable of giving compositional and structural information as a function of depth with a substantially improved depth resolution [12-15]. The energy of the scattered ion depends on the mass of the nucleus it collides with, modified by the inelastic energy loss on its incoming and outgoing trajectories.

For a crystalline target e.g. Si, the number of scattered ions at a particular angle depends not only on the Rutherford-like scattering cross section but also on channeling and blocking effects. Typically in MEIS, the ion beam is aligned with a major crystallographic axis resulting in the shadowing of deeper lying Si atoms by surface atoms and this makes the technique highly surface specific. Ions scattered from the lower layers will have their outward paths blocked at certain angles by upper layer atoms. The variation in scattered ion intensity with angle thus relates to the geometrical arrangement of surface atoms and has been extensively exploited to perform surface crystallography studies [13, 16], which is an area not discussed further here. However in the case of analysis of nanolayers deposited on Si, the so-called double alignment configuration applied prevents scattering information from deeper into the underlying crystalline matrix from being recorded.

Data is collected in the form of a 2-D spectrum of the backscattered ion yield as a function of both energy and scattering angle. When using double alignment conditions energy spectra are obtained by making a cut through the 2-D spectrum at a fixed exit angle (the blocking direction). The spectrum thus obtained can then be converted into quantitative depth profiles of most species present in, say, the first 30 nm layer/surface depth, for nuclei with a mass as low as carbon [17].

The energy of a backscattering peak in the spectrum is related to the depth at which a collision took place and is the result of both elastic and inelastic energy loss processes. The conversion of the energy scale into a depth scale depth relies on an accurate knowledge of the inelastic energy loss rates (dE/dx), which are well documented [18,19]. When considering a single species such as e.g. a semi-dilute implant of a heavy mass X in Si, this is comparatively straightforward [15]. However it becomes substantially more complex and cumbersome in the case of the analysis of

multilayers, especially when the layers have strongly different energy loss rates and this then requires spectrum simulation [20] in order to extract the maximum amount of quantitative information.

For a heavy species X in Si system mentioned, the conversion of scattering yield to concentration is normally achieved through an internal calibration by comparing the yield obtained with that from an amorphized Si sample, taking into account the squared ratio of the scattering cross sections for Si and X ($\propto (Z_{Si} / Z_X)^2$, where Z is the atomic number) [21]. This procedure assumes that the cross sections for scattering at these medium energies are Rutherford-like, which however is strictly incorrect since electron screening of the nucleus still occurs. This deviation can be accounted for by applying a screening correction.

The cross section correction applied is due to Andersen [22] and this is combined with a second correction that accounts for the degree of neutralization of the He particle when emerging from the sample surface. This neutralization (ionization) correction is important since only charged particles are analyzed in MEIS. It is based on a collation of experimental charged fractions data obtained on a wide range of targets measured at the FOM Institute for both H and He ions [23] and results by Kim et al. [24] for H ions, indicating that these charged fractions primarily depend on the analyzed energy, although it must be mentioned that Kido et al. [25] have found deviations on very clean surfaces. Through the application of both these corrections it is now considered that MEIS can determine the concentration of most species with an accuracy of better than 5% [26] as will also be demonstrated in this study.

The ability of MEIS to obtain a depth resolution of better than 1 nm near the surface, (which however deteriorates with increased depth due to straggling) is due to a combination of the use of a high energy resolution electrostatic energy analyser (0.35%) [12], the operation at an ion beam energy not far removed from the maximum in the inelastic energy loss rate curve (100-200 keV) [18] and the use of longest possible path lengths of the particle inside the layer through an optimum choice of the scattering geometry. The precision of the depth determination of a scattering event, as used in a layer thickness measurement, is better than 0.2 nm, while its accuracy depends on the accurate knowledge of the inelastic energy loss rates used in materials, which, as mentioned above, are well documented. This ability makes MEIS a valuable characterization tool of dielectric films of nanometer thickness [14, 20, 26-29], ultra shallow implants [15, 17] etc. As referred to above the technique has been extensively used for the characterization of the registry, relaxation and expansion of sub-monolayer (and monolayer) overlayers of species on single crystal surfaces, the growth thereof as well as inter-layer diffusion effects [13,16].

3. Energy spectrum simulation

The interpretation of MEIS energy spectra from multilayers is complex and requires spectrum simulation as mentioned.. The simulation model used operates as a macro within the IGOR© graphing package [30] and was developed at Daresbury

Laboratory [31]. It has been described in more detail in [20] and only a very brief outline is given here. On the basis of layer growth parameters or information from the spectrum, a model layer structure is assumed. In the simulation this layer structure is sliced into, say, 0.1 nm wide layers and the scattering contributions of the fractions of the different masses in each slice to the energy spectrum are calculated as Gaussian distributions, the heights of which are proportional to the cross section, modified by the two corrections mentioned above and their widths increased for greater depths to account for depth dependent straggling. Energy (and depth) dependent inelastic energy loss rates, obtained from SRIM [19] using best known compound densities are used in the model for different layer compositions. A changing composition near an interface due to e.g. interdiffusion, alters the stopping in each successive slice which is calculated by applying Bragg's rule using the local composition. The contributions of all slices are added up and finally normalized at the surface typically over the top 2-3 nm (bookkeeping). The best layer structure is obtained by iteration giving the best match with the experimental spectrum, based on a X_{min}^2 test. A change of the layer thickness by 0.1 nm from the best fit result in the simulation model clearly shows a visibly worse spectrum match and hence the precision of the thickness determination of layer with a sharp interface can be said to be easily better than 0.2 nm.

4. Sample preparation and experimental conditions

All layers reported on here were produced at IMEC on 300 mm Si(100) wafers prepared using the IMEC clean [32], which causes the removal of the native oxide and growth of a ~1 nm SiO_2 layer.

The first set of samples were Hf based and consisted of nominally 2 nm thick, HfO_2 or $Hf_xSi_{1-x}O_2$ (60% Hf) layers that were deposited by MOCVD on cleaned Si(100). The effect of nitridation at 800°C on the depth profiles, using a decoupled plasma nitridation process (DPN) (Applied Materials) was also investigated since the thermal stability and electrical behaviour of these materials may be improved by plasma nitridation.

Complete TiN/STO/TiN MIMcap layer structures on Si wafers were produced and the effect of adding each layer investigated by MEIS. TiN top and bottom layers nominally 2 and 3 nm thick, respectively, were grown in a PVD process (Anelva) by sputter deposition from an elemental titanium target in a Ar/N_2 mixture. The STO layer was grown by ALD (ASM Pulsar) nominally 3 nm thick, using a Sr:Ti pulse ratio of either 4:3 or 3:1 to form either a stoichiometric STO layer, or a Sr-rich STO layer, respectively, and the effect of thermal annealing (RTA) at 650 °C for 15s was studied. Further details are given in [7,10]

Finally the TiO_2/Ru layer based MIMcap structures investigated were again grown using a nominally 3 nm TiN bottom layer grown by PVD on cleaned 300 mm Si(100) wafers, followed by a 3 nm Ru layer deposited by using plasma enhanced ALD (PEALD) [9, 33] followed by ALD growth of the crystalline dielectric TiO_2 (rutile) at 250 °C using O_3 as oxidant after the insertion of a sub nm of an oxidized Ti

interlayer using H_2O as oxidant which avoids later Ru etching by O_3 leading to unacceptable interface roughness [34].

Samples of 12 x 12 mm for MEIS analysis were cut from these wafers under clean conditions. For each layer system a range of samples were investigated in which the effect of changing a growth or processing parameter could be studied. Of the range of nanolayers and structures investigated only the results of selected samples will be presented here.

MEIS experiments were performed at the Daresbury Laboratory MEIS facility [16] in UHV using 100 or 200 keV He^+ primary ions. Double alignment conditions were employed for all samples, leading to a major reduction of the scattering from the underlying Si matrix. Scattering angles were chosen for each sample system to give optimum mass, depth resolution and scattering yield. In all cases the incident beam direction was aligned with the [-1-11] channel. For the Hf based samples He ion energy was 100 keV and the detector aligned with the [111] blocking direction, giving a scattering angle of 70.5°. Although the near-surface depth resolution for these conditions is better than 0.8 nm, as based the slope of the leading edge of the Si peak recorded on a clean Si surface, this quantity deteriorates with depth as it is due to both the system energy resolution and straggling, with the latter increasing with depth. Parts of the spectra containing the peaks due to low masses (e.g. N, O) were recorded 2-4 times with a corresponding higher ion beam dose compared to the heavier mass part of the spectrum, and then averaged. Energy spectra were extracted from these 2-D spectra. For the STO/TiN and Ru/TiO_2 layers investigated the scattering angle was increased to 90° through the use of the [221] blocking direction, and for the latter system the ion energy increased to 200 keV in order to optimise the peak separation in the spectrum.

5. Results and Discussion

Hf based nanolayers

The starting surface in the samples studied was the IMEC cleaned Si(100) surface which has a nominally 1 nm thick protective SiO_2 layer. This layer and the effect of DPN at 850° C was initially investigated with MEIS and the results obtained [20] are briefly mentioned first. From the simulation of the energy spectrum recorded it is found that the as deposited layer has a thickness of 1.2 nm, close to the nominal value, in excellent agreement with XPS and Spectroscopic Ellipsometry (SE) measurements on samples cut from the same wafer [35, 36]. Nitridation leads to the appearance of a clear, well resolved N peak in the spectrum the result of a N fraction of ~18% at the oxide interface, which correspondingly lowers the O fraction in the oxide, but which drops off towards the surface due to reoxidation upon exposure to the air. DPN causes N penetration to a depth of ≥ 2 nm and also the drive-in of the O atoms. Before DPN treatment of the oxide, only the top Si atoms of the Si matrix are visible (due to shadowing). Afterwards the depth of the “visible” Si has increased by

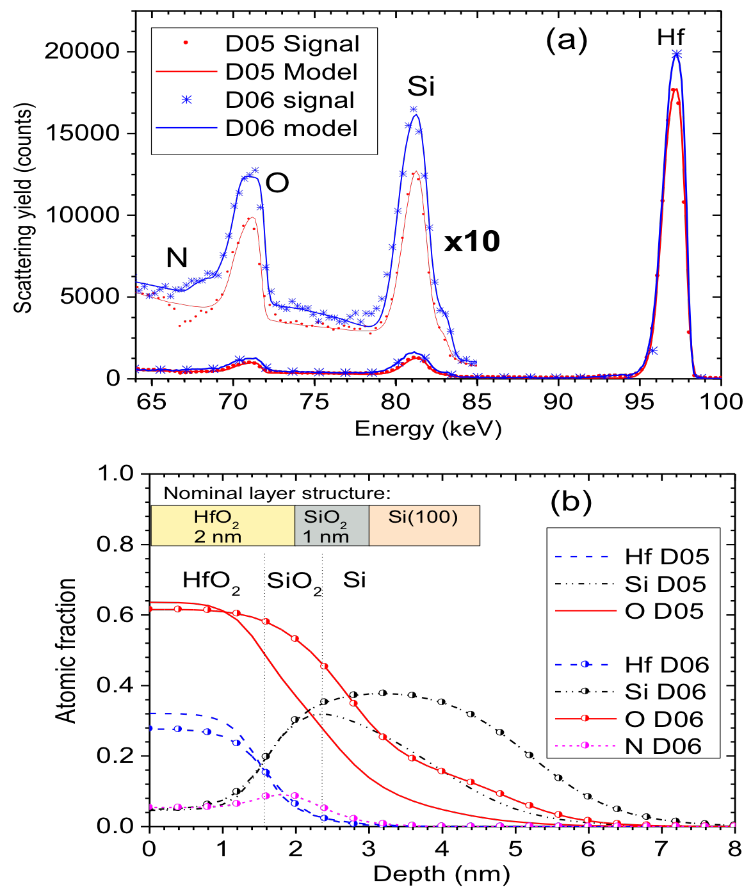

Figure 1. (a) Energy spectra and model simulations and (b) derived depth profiles for layers D05 ($Si/SiO_2/HfO_2$) and D06 ($Si/SiO_2/HfO_2$/DPN) including the nominal layer structure.

around 0.5 nm clearly indicating that the plasma treatment causes some deeper Si disordering.

MEIS spectra obtained after the addition of a nominally 2 nm HfO_2 layer on top of the starting oxide both before (D05) and after DPN (D06) are shown in Figure 1a (data points) including the best fit model simulations (lines). Peaks due to scattering of different species are annotated. Figure 1b shows the depth profiles derived and here, as in all figures of depth profiles presented in this work, a schematic of the nominal initial layer structure is shown. The inelastic energy loss rates used for the depth of the profiles were calculated by SRIM [19], assuming bulk densities of 2.2 g/cm^3 for SiO_2 while for HfO_2 two different values, i.e. 9.7 (bulk) and 8.7 g/cm^3 were used since film densities reduced by ~10 % from the bulk value have been observed for very thin films [28]. For the Hf silicate layers discussed later in this section the simulation applies Bragg's rule to calculate the electronic stopping rates. Analysis of the simulations shows the composition for the D05 and D06 samples to be stoichiometric to within a few % and their thicknesses to be 1.6 and 1.5 nm assuming bulk densities, or 1.75 and 1.65 nm assuming a 10 % lower thin film density, respectively, before and after DPN. Thicknesses are determined by the half heights of the profiles and are layers are marked in Figure for sample D05 assuming bulk density. Whilst the composition of the HfO_2 is as expected, the thicknesses determined by MEIS are less than the nominal value of 2 nm. It should be mentioned that thickness measurements of samples from this wafer made by SE, XPS, XRF and XTEM, closely confirm the MEIS result [35, 36], and thus support its accuracy. Based on the best fit in the

simulation model, DPN causes a small N peak in the spectrum representing a ~5 % N content in the HfO_2 layer, somewhat increasing into the underlying SiO_2 layer and, a corresponding small reduction of the O content in the oxide layer. A small reduction of the Hf level is also seen in both the spectrum and the simulated depth profile. The increase of the N level deeper in (the SiO_2 layer) is not dissimilar to that found in the DPN treatment of the SiO_2 layer mentioned above. Commenting briefly on the sudden drop in signal starting at ~66.5 keV up to ~68.5 keV, this is due to a very occasionally occurring loss of signal in a MEIS experiment to below the near linear dechanneling background to which the experimental data normally corresponds. The determination of the N content in D06 is not likely to be affected by the dip since was made on a different sample for which the normal situation of a near straight background, as given by the model simulation, was assumed. It is also seen that the high-energy (surface) side of the O peak in the as deposited sample D05, is less steep than the simulation. This probably caused by hydrocarbon contamination, not easily measured in MEIS but clearly seen in XPS [36], which can broaden up-slope of especially the O peak. Looking at the depth profiles, sample D05 shows an O signal with a decaying part that extends 0.8-0.9 nm beyond the Hf one and this allows an estimate to be made for thickness of the SiO_2 layer which is somewhat reduced from the 1.2 nm found for the starting oxide. It is worth noting that MEIS shows the presence of 5-6 % Si in the Hf layer of both samples, as evidenced by the high-energy shoulder on the Si peak at ~83 keV. At first sight it is curious that the apparently higher Si shoulder in D06 is not immediately reflected in the simulated depth profile but it is possibly associated with the "bookkeeping" to ensure that in the surface region the fractions add up to one. Combined with the observation of the reduction in thickness of the oxide layer in sample D05, the low level "presence" of Si in the Hf suggests the possibility of some SiO_2 being consumed and incorporated into HfO_2 layer during the deposition. On the other hand, the presence of pores in these ultra thin layers cannot be excluded. Consistent with the finding mentioned above for the SiO_2 sample after DPN, the greater depth of the Si profile in Figure 1b shows that DPN again has caused an increase in the depth of the disorder by ≥1nm in the Si lattice as well as some drive-in of the oxygen. The increased heights of the Si and O peaks in the spectrum of sample D06 are associated with the increased width of the layers visible in MEIS after DPN and possibly some reoxidation. XTEM analysis of a sample from this wafer shows that the HfO_2 layers contains microcrystallites after annealing at 800°C and that the layer interfaces are comparatively rough [35].

Spectra obtained both before (D07) and after DPN (D08) for a nominally 2 nm thick $Hf_xSi_{1-x}O_2$ (60% Hf) layer deposited on SiO_2 are shown in Figure 2a, together with best fit spectrum simulations. The corresponding models are shown in Figure 2b. The Si/Hf ratio determined by MEIS is 60 % within 2 %, in agreement with the growth parameters. Layer thicknesses measured for sample D07 are 1.4 nm (for 6.7 g/cm^3) or 1.5 nm (for 6.1 g/cm^3) (as marked in Figure 2b) and for D08 1.75 nm and 1.6 nm for these two densities. While agreement with XRF and XTEM measurements on these samples is within 10 %, XPS yields values ~20% higher [35,36]. The thickness of the SiO_2 layer based on the half heights of the Hf and O signals in Figure

2b is 0.8 -1 nm. The changes due to DPN at 800 °C are evident. The amount of N in the SiO_2 layer is up to 10% reducing to 4 % in the silicate layer. Observations made above on the increase in depth of the Si disorder and O drive-in following DPN apply here too. It is worth mentioning that XTEM observations of these samples show the

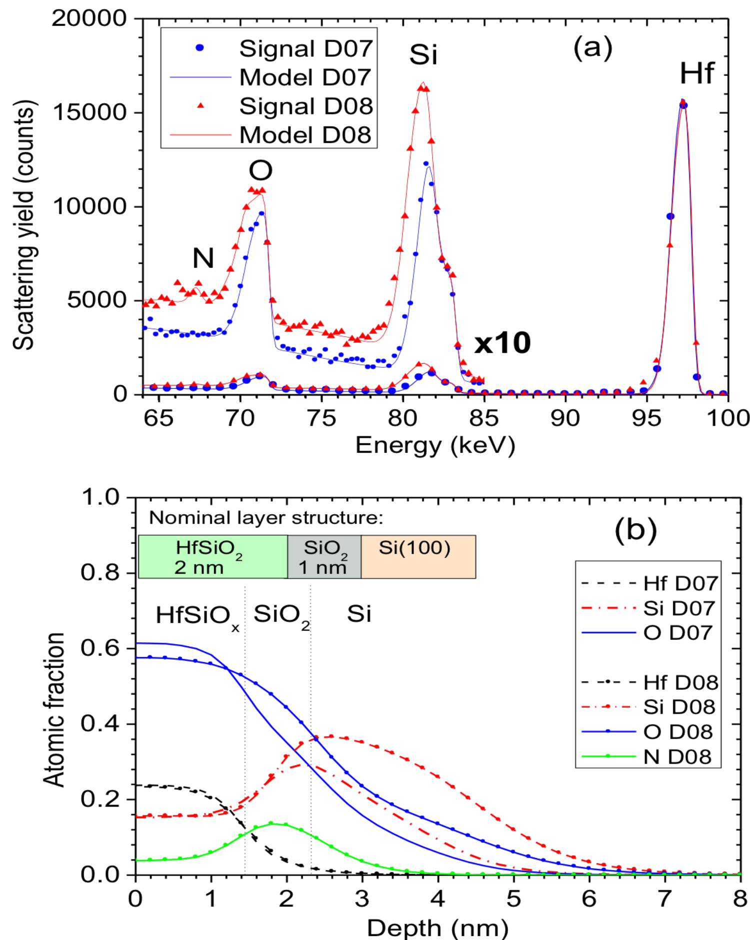

Figure 2. (a) Energy spectra and model simulations and (b) derived depth profiles for layers D07 (Si/SiO_2/$HfSiO_x$ (60%Hf)) and D08 (Si/SiO_2/$HfSiO_x$ (60%Hf)/ DPN) including the nominal layer structure.

absence of recrystallization in these Hf silicate samples as well as the smoothing of the interfaces following DPN [35].

A final example in this section of the capability of MEIS is its application to the analysis of a complex ~7 nm wide, hafnia based high-k / metal gate (HKMG) multilayer stack with the following nominal structure, schematically shown in Figure 3b: TiN(3nm) / Al_2O_3(0.9nm) /HfO_2(2nm) / SiO_2(1nm) / Si. This structure represented a challenge for the MEIS technique as well as the simulation model and the underlying SiO_2 /Si layers were not included in the simulation. The purpose of the insertion of thin Al_2O_3 layer in this stack was to effect a modification of the workfunction (WF) of the metal gate [37] after annealing to 1025°C. The cause of this change could be related to a compositional modification of the high-k/metal interface and depth profile analysis of the constituents might elucidate the changes taking place. Samples were analyzed before (D13) and after annealing in an inert gas atmosphere

(D14) using MEIS in addition to TOFSIMS and ARXPS [36]. Energy spectra with the different scattering peaks annotated, together with best fit sample structures before and after annealing, are shown in Figures 3a and b. The simulated film structure before annealing, confirms the as-grown film layer parameters quite accurately as marked in Figure 3b: 3 nm TiN (surface oxidized) on top of 0.9 nm AlO_x and 1.7 nm HfO_2. The most significant observation in the energy spectrum after annealing is the shift of the Hf peak by about 1 keV towards higher energy. In the depth profiles this is

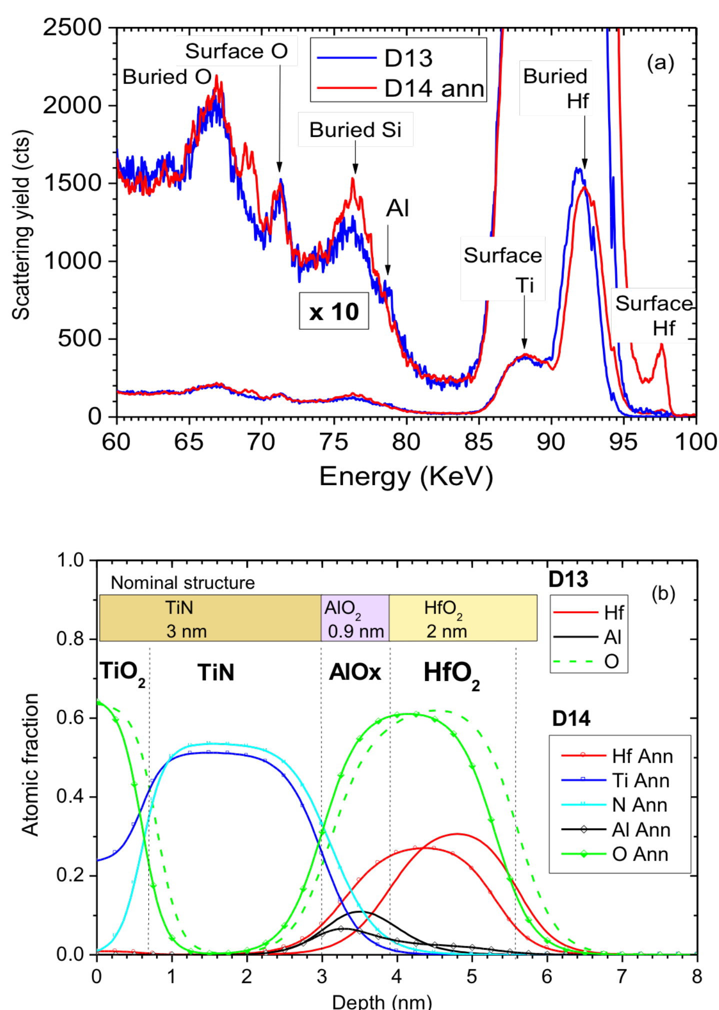

Figure 3. (a) MEIS energy spectra (b) and derived depth profiles of a nominal TiN(3nm)/ Al_2O_3(0.9nm)/ HfO_2(2nm)/SiO_2(1nm)/Si metal gate high-k layer stack (schematically shown), showing Hf and Al interdiffusion, upon annealing.

reflected as a shift of the Hf (and O) profiles towards the surface, in the case of Hf by ~0.4 nm, i.e. a move of Hf into the original AlO_x caplayer. Note that the back edge of the TiN layer however remains unchanged. Since the anneal did not change the Ti and N distributions, only the post annealing Ti and N profiles of sample D14 are shown for clarity. The movement of Hf implies a reverse Al diffusion into the Hf oxide layer and this is indeed seen in the simulation in the Al profile that as a result has reduced in height. This observation is in agreement with TOFSIMS results [37] and confirms

that compositional changes occur at the interface that could be associated with the observed change in workfunction. Although depth profiles recorded by TOFSIMS demonstrate low level Al diffusion into the TiN layer [37] and indeed some Al surface segregation, this level is below the sensitivity of MEIS. Finally it is interesting to note that the post annealing MEIS spectrum shows that this treatment results in a ~1% Hf segregation at the surface as indicated by the surface Hf marker.

TiN/STO/TiN nanolayers

In this section the MEIS spectra are presented and discussed of samples after the various stages of depositing the individual layers required for the build up of a complete TiN/STO/TIN MIMcap layer structure onto a cleaned Si wafer. In particular the effects of rapid thermal annealing (RTA) at 650 °C for 15s is considered. Figure 4a shows the MEIS spectrum and model simulation after deposition of a nominally 3 nm thick TiN layer (sample D02). The different annotated peaks are well separated and the quality of the fit is good. The narrow O peak observed indicates the presence of a thin surface oxide. Derived depth profiles are shown in Figure 4b. They show the

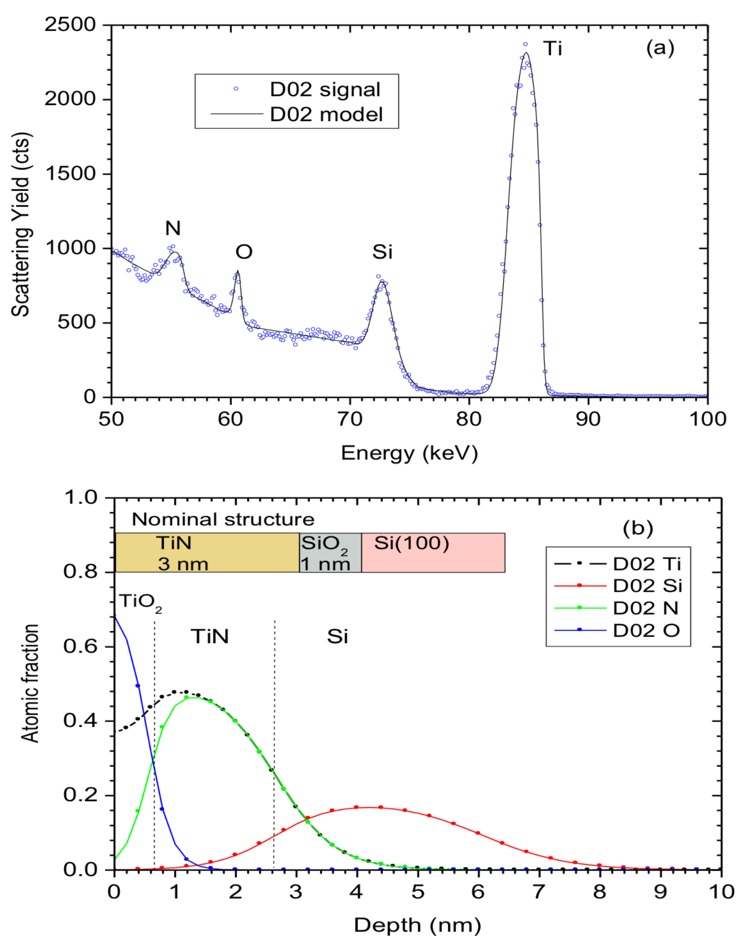

Figure 4. (a) MEIS energy spectra and model simulations and (b) simulated depth profiles for sample D02 (Si/TiN) including the nominal layer structure.

presence of a stoichiometric TiN layer that however has a deficit of N near the surface due to reoxidation following exposure at the air. As marked in Figure 4b, the depth of the TiN layer (based on the half-heights of the Ti and N downslopes as well as the Si upslope) is measured as 2.6 nm, below the nominal value. This compares with a value of 3.3 nm determined using XPS on the same sample [39]. There is no evidence in the MEIS spectrum of any O signal from below the TiN layer; on the other hand Si disorder extends to a depth of ~ 6 nm which compares with a disordered layer of ≤ 3 nm for the as cleaned Si surface. These observations show that the TiN PVD sputter deposition process not only removes the thin oxide layer but also affects the crystallinity of the underlying silicon. The observation of sputter damage is confirmed by XRR measurements made at IMEC that show the formation of a shallow damage layer [38].

The changes to the energy spectra due to the addition of a 3 nm Sr-rich STO layer to the 3 nm TiN bottom layer are seen in Figures 5a in the presence of a Sr peak and appearance of a high energy shoulder to the Ti peak, with the latter representing the Ti in the STO layer. The difference due to thermal processing at 650 °C for 15 s is visible when comparing the spectra of samples D05 (before) and D06 (after). Sr rich STO layers can be deposited by changing the Sr to Ti precursor pulse ratio during ALD growth with high Sr/(Sr+Ti) ratios resulting in an increased recrystallization temperature of the layer [7]. The 3:1 pulse ratio applied for producing samples D05 and D06 results in a Sr/(Sr+Ti) ratio of 0.62 as measured by RBS on 20 nm thick samples, while a 4:3 pulse ratio is found to lead to stoichiometric STO (Sr/(Sr+Ti) = 0.5) [7]. Depth profiles obtained for samples D05 and D06 are shown in Figure 5b, including a schematic of the nominal structure.

Although the fit of the model simulations to the MEIS signal in Figure 5a is good it must be mentioned that the silicon peak between 69 and 74 keV is not included in the simulation as the simulation model can currently only process up to four elements simultaneously. The energy spectrum was therefore first modelled excluding the silicon peak, which was then 'folded in' in a second stage simulation (providing an excellent fit to the experimental Si peak) and thus the Si profiles are also presented in Figure 5b. Since Si is the deepest layer this folding in does not affect the spectral peaks due to the layers closer to the surface.

The first point to note from the energy spectrum is that the Sr peak due to the Sr rich STO layer before annealing (D05) is unusually sharp at the high-energy edge. This shows surface Sr segregation, as also confirmed by ARXPS measurements [38] which is probably a monolayer of Sr in the form of SrO/SrOH and $SrCO_3$ [39]. This enrichment is not seen in MEIS spectra recorded on stoichiometric STO (not shown) which is itself also less affected by annealing i.e. is thermally more stable. Annealing to 650 °C for 30 s causes three notable changes in the spectra, i) a loss of Sr by more than 10 %, especially the segregated fraction, resulting in a more normal rounded peakshape; ii) an increase in the Ti content in the STO layer as evidenced by the increase in the Ti signal in the shoulder around 85 keV by a similar amount and iii) a small shift of the Ti peak to higher energies, i.e. closer to the surface. In the model simulations the density values for STO before and after annealing were taken as

determined by Menou et al. [7] as, respectively, at 85% and 95 % of the bulk value of 5.12 g/cm^3. From the derived depth profiles it is concluded that before annealing (sample D05) the Sr/(Sr+Ti) ratio is 0.6 at the half depth of the STO layer (away from the effect of surface segregation) which agrees well with the RBS measurement of 0.62 made on a 20 nm thick, 3:1 pulse ratio STO layer [7]. After annealing (sample D06) the ratio is reduced to 0.55 confirming strontium loss during the annealing process and showing a change in stoichiometry. It is worth mentioning that for the similar layer structure of stoichiometric STO on TiN any such change was insignificant.

Before annealing the thickness of the STO layer, as based on the half heights of the Sr, Ti, O an N profiles all of which closely coincide, is measured as 3.3 nm, 10% above the nominal value. That of the TiN layer measured similarly, is 2.9 nm in close agreement with the nominal value of 3 nm. Layers are marked in Figure 5b. XPS measurements on these samples yield ~10% higher values for these thicknesses [39]. The N depth profile appears to extend ~0.8 nm beyond the titanium into the silicon, however the accuracy of the N peak position is not high as it is affected by its low counts and accuracy of background subtraction in this part of the spectrum. After annealing the width of the Sr profile is marginally reduced to 3.2 nm (in part due to

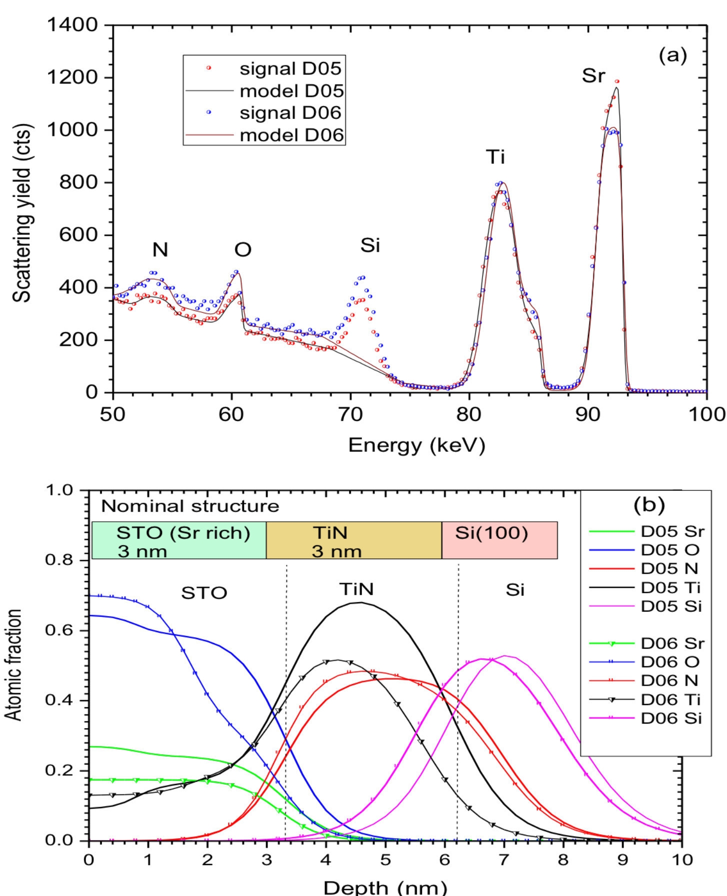

Figure 5. (a) MEIS energy spectra and model simulations and (b) simulated depth profiles for samples D05 (Si/TiN/Sr-rich STO) and D06 (Si/TiN/Sr-rich STO 15s 650°C), including the nominal layer structure.

the change in density) and that of the TiN layer to 2.6 nm in correlation with the narrower Ti peak noted above. Corresponding values by XPS are 3.4 and 3.2 nm, respectively [39]. The O scattering peak is visibly narrower after annealing which is reflected in the O depth profile that is narrower than that of the STO layer and this is not wholly understood. Its increased height may suggest a degree of O enrichment in the STO layer after annealing. On the other hand normalisation of the depth profiles to 100% is performed over the first 2-3 nm and narrow surface peaks can introduce a degree of distortion in the atomic fraction.

The final MEIS analysed samples considered in this section are full MIMcap multilayer structures: a 3 nm TiN bottom layer followed by a 3 nm stoichiometric STO dielectric layer capped by a 2 nm thick TiN top layer both before (D11) and after (D12) annealing (RTA) to 650 C for 15 s. The energy spectra and simulations are shown in Figure 6a and the derived best fit profiles in Figure 6b which also contains the nominal layer structure. The highest energy Sr peak at 91 keV is due to the STO layer sandwiched between two TiN layers that result in two Ti and two N peaks. The O peak at ~58 keV is due to the STO layer and the narrow O peak at ~61 keV to surface re-oxidation of the top TiN layer. Interestingly, a small Sr peak is seen at 93

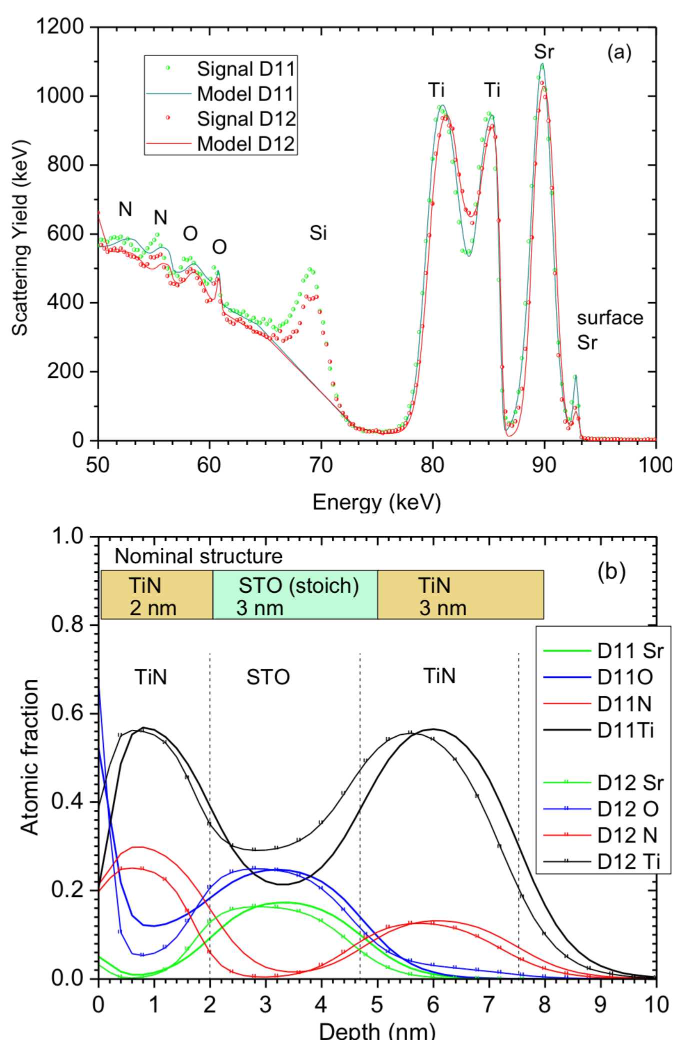

Figure 6. (a) MEIS energy spectra and model simulations and (b) simulated depth profiles for samples D11 (Si/TiN/stoich STO/TiN) and D12 (Si/TiN/stoich STO/ TiN, 650°C 15s) shown schematically.

keV which derives from a small amount of segregated Sr on top of the top TiN layer, an effect also noted in Figure 3a for Hf/TiN. It is reduced after annealing. A narrow, 0.2 nm wide surface layer is required to model this Sr peak which equates to only a few atomic % of Sr. Believed to consist of SrO/ SrOH/$SrCO_3$ as noted above, it also accounts for the narrow O peak and the sharp O profile in Figure 6b. From a processing point of view the most significant change in the spectrum after annealing is the increase in the Ti signal at ~84 keV showing the increased Ti content in the STO layer which is matched by a similar reduction in the Sr fraction as shown by the lower height of the Sr signal at 90 keV. MEIS analysis clearly confirms interdiffusion between the STO and TiN layers due to annealing.

Although the fit of the simulated energy spectra is good for the Sr, Ti peaks, it less so for the O and worse for the N peaks. Another observation is the substantially lower count in the N peak from the bottom 3 nm wide TiN layer compared to the top one which is surprising and not understood. These peaks convert into depth profiles in which the levels of the N fractions are not realistic in that they are too far removed from 50 % as they would be expected to be. This observation might raise the issue of whether the degree of neutralisation of the He ion backscattered from deeper layers is correctly described by the empirical correction mentioned in Section 2. On the other hand results from a deep TiN layer the next section give no reason to question this approach. The actual reason is believed to be a present limitation in the normalisation procedure which in this sample is affected by the high O spike near the surface. Despite these aspects the layer thicknesses measured by MEIS are in excellent agreement with the nominal values, with the top TiN layer at 2.0 nm, the STO layer at 2.9 and the bottom TiN layer at 2.9 nm all of which are unchanged after annealing although as shown above, there is clear diffusion across the interfaces between these layers.

TiO_2 /Ru /TiN nanolayers

The dielectric TiO_2 is an attractive alternative to STO as a MIMcap material in view of its thermal stability, low cost and already wide industrial application. The preferred rutile crystalline phase which has a *k* value of ~ 90, may be grown by ALD using O_3 as the oxidant on tetragonal RuO_2 which is likely to act as a template due to its close lattice match. [8,40]. An added attraction of Ru is the fact that RuO_2 is a conductor and as such does not add to the EOT of the dielectric. The use of H_2O as oxidant during ALD is found to lead to the growth of the anatase TiO_2 phase which has a lower *k* value (~40) [8]. The exposure of Ru to ozone to form RuO_2 however causes etching and Ru loss (due to volatile RuO_4 formation) leading to an increased roughness and worse electrical behaviour [9]. However it was found that the initial deposition of TiO_2 using H_2O as oxidant to a thickness of ~0.3 nm appears to form a protective layer, largely resistant to etching and Ru loss during later O_3 mediated TiO_2 growth.

Detailed analysis of the layer growth rate by Popovici et al. [34] suggest the possibility of the formation of a mixed phase $RuTiO_x$ interlayer that protects against etching even for sub-ML TiO_2 growth with H_2O as the oxidant. Indeed TOFSIMS

analysis shows a higher Ru and Ti interdiffusion for H_2O mediated TiO_2 growth compared to O_3 and XTEM studies also confirm the existence of a ~1.4-1.7 nm wide contrast layer in the micrographs that may relate to the formation of an interlayer [34].

MEIS depth profiling using 200 keV He^+ ions and a scattering angle of 90° has been applied to such a layer structure with the aim of whether it could confirm the formation of any interlayer. The layer structure consisted of nominally a 3 nm thick TiN bottom electrode underneath a nominal 3 nm Ru layer, exposed to 3 cycles of TiO_2 (H_2O) growth, and then covered with a 3 nm TiO_2 (O_3) layer. The energy spectrum including spectrum simulation (with the Si peak again excluded) is shown in Figure 7a with the peak origins indicated. Note that in addition to peaks due to scattered He^+ ions, the spectrum also contains those due to backscattering of He^{++} ions. The obtained depth profiles of the constituents from the MEIS spectrum are given in Figure 7b. Below the TiO_2 toplayer of 4.3 nm thickness, a 1.8 nm thick layer

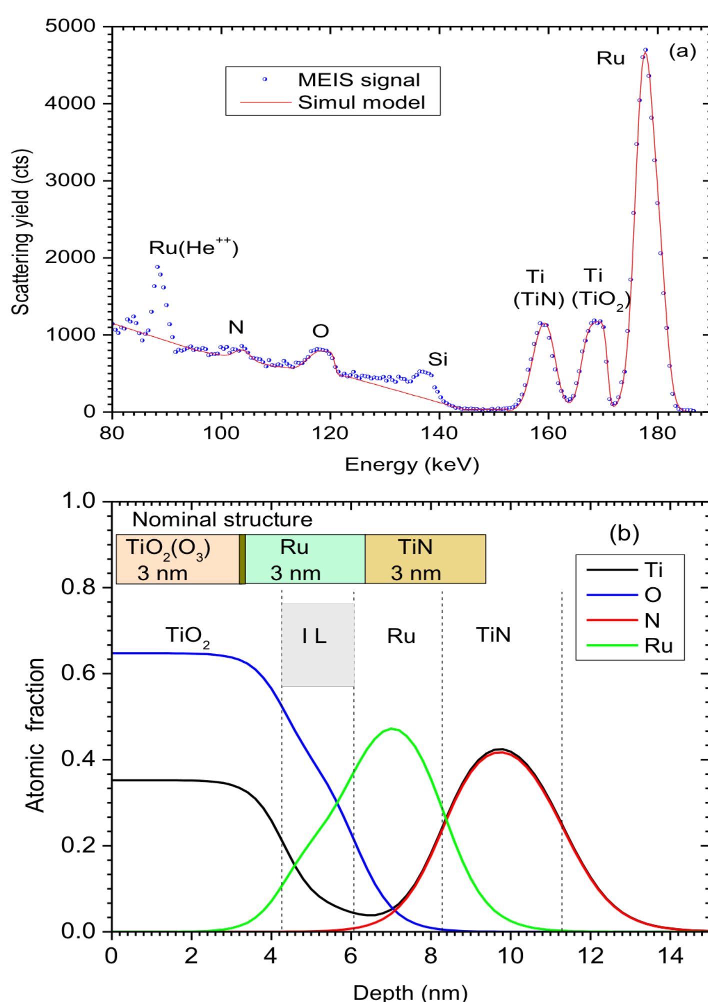

Figure 7. (a) MEIS energy spectra and model simulations and (b) simulated depth profiles for the (Si/TiN/Ru/TiO_2) layer structure, shown schematically. The interlayer containing Ti, O and Ru is indicated.

containing Ru, O and Ti is seen, followed by a 2.2 nm thick Ru layer on top of a 3 nm TiN layer. The different layers identified are again indicated in the figure. In view of the object of this analysis, a significant observation is that the Ti peak (due to TiO_2) and the Ru peak have slopes, at lower and higher energies compared to their maxima, respectively, that are considerably less steep than typically encountered for sharp interfaces. This observation confirms the occurrence of substantial interdiffusion between the layers. The width of the interlayer developed is found to be 1.8 nm in close accord with that found in XTEM mentioned above. MEIS analysis thus appears to confirm the formation of a mixed interlayer containing Ru, O and Ti as suggested [34] which has a composition roughly in a ratio of 2: 4: 1. It has to be emphasised that this ratio is very approximate as for one thing the Ru peak, because of the small width of the layer does not reach 100%. With regard to the TiO_2 layer, the stoichiometry is (0.54:1), close to that expected and that of the bottom layer is 1:1 (profiles coincide). Thus the problem encountered with the apparent low N level in the previous section is not found here despite the depth of the layer being greater than 8 nm. Hence the problem with the N profile seen above is not a generic problem.

The final example is a layer structure largely identical to the previous sample but for the fact that the TiO_2 is doped with 1% Al for the purpose of reducing the leakage current density of the MIMCAP stacks [41]. The layer structure was annealed in Ar for 60 s at 370 °C and the issue of interest was the fate of the Al dopant upon annealing. The low Al level in the sample certainly presents a challenge for MEIS. Figure 8 shows the energy spectrum and simulation with the region in which the Al is expected to occur shown in the inset with a 10 x expanded yield scale. A small peak is indeed seen at ~ 148 keV which is unambiguously confirmed to be Al in the original 2-D spectrum where it shows the expected angular dependence. The model simulation (solid line) used assumes that 1% Al is uniformily distributed in the TiO_2 layer. As the inset shows this is clearly not confirmed by the experimental data and indicates

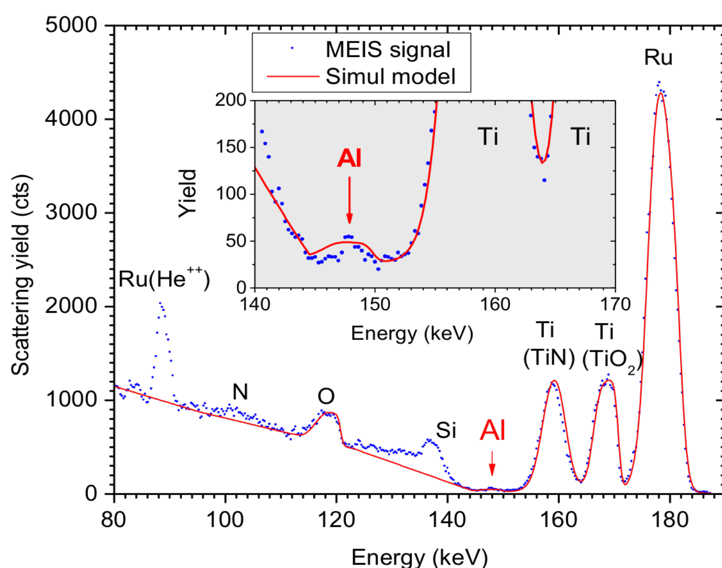

Figure 8. Energy spectrum and model simulations of a (Si/TiN/Ru/TiO_2 -1%Al, 370°C, 60 s) layer structure. The Al peak occurs at around 148 keV as shown in the inset. Al is seen to have segregated towards the top of the layer after annealing.

that the Al has segregated towards the top of the TiO_2 layer. Despite the low level of the Al dopant, MEIS is able to extract this information with high depth resolution.

6. Conclusion

MEIS analysis for the determination of composition depth profiles and structural information of nanolayers is briefly described and relevant aspects of the technique considered. Quantification requires the performing of spectrum simulation using a model that correctly accounts for straggling, energy and composition dependent stopping and includes cross section and neutralization yield corrections. The application of the technique to a range of high-k nanolayers and structures relevant to advanced CMOS developments demonstrates the capability of MEIS i) to measure layer thickness with good accuracy (≤ 0.2 nm), ii) to determine layer composition /stoichiometry in good agreement with growth parameters or alternative techniques, and iii) to monitor changes in composition and depth profiles, especially interdiffusion and segregation following thermal or plasma processing.

With regard to HfO_2 or $Hf_xSi_{1-x}O_2$ layers investigated, MEIS analysis indicates the consumption of some of the underlying SiO_2 during HfO_2 deposition and the apparent Si incorporation at low (5%) level into the grown HfO_2 film. N uptake and profiles in these layers following plasma nitridation (DPN) were determined. DPN was found to cause an increase in disorder in the Si lattice to a depth of ≥1 nm as well as a drive-in of O from the oxide. MEIS applied to characterization of a complex high-*k*, metal gate (HKMG) layer structure confirmed the as grown film parameters but significantly, showed the diffusion, after thermal treatment at 1025 °C, of Hf into the Al caplayer inserted to adjust the metal gate workfunction and Al into the HfO_2.

In relation to the analysis of samples of each of the stages of the build up of the full TiN/STO/TiN MIMcap structure, MEIS shows that the deposition of TiN on SiO_2/Si by the PVD process leads to the removal of the oxide and production of a disordered layer in the underlying Si matrix to a depth of 6 nm. Sr rich STO layers deposited on TiN are shown to have considerable Sr segregation at the surface, not seen in stoichiometric STO, which is probably in the form of SrO/SrOH/$SrCO_3$ as supported by the evidence of a narrow O layer. Annealing to 650 °C removes the Sr surface enrichment and changes the stoichiometry. From a processing point of view a significant observation in the analysis of the full MIMcap structure is the clear interdiffusion between the TiN and STO layers following annealing.

Finally, a MEIS analysis of an overall ~10 nm wide TiO_2 /Ru /TiN nanolayer system was made to investigate if it could confirm the possible formation of a mixed interlayer during H_2O mediated ALD growth of TiO_2 on Ru during a first few cycles which preceded the ALD deposition of the actual TiO_2 layer mediated by O_3 and protected Ru against etching by O_3. MEIS depth profiling identified extended interface slopes between the two layers of the structure and in particular the presence of a 1.8 nm wide layer of mixed Ru, O and Ti composition, which confirmed XTEM

and TOFSIMS results and supported the hypothesis. The same layer structure but with a 1% Al doping in the TiO_2 layer was also investigated and MEIS was able to show the apparent segregation of Al towards the top of the TiO_2 layer upon annealing at 370 °C for 60 s.

In MEIS analysis of nano layers grown on Si, the facility of being able to choose the ion energy as well as the scattering configuration (albeit from the limited number of blocking directions available) offers a degree of flexibility that allows optimum peak separation with acceptable sensitivity to be selected. Although the technique has its limitations, e.g. its sensitivity to light ions and mass resolution for high masses, and some uncertainties as yet remain in aspects of the simulation model, it can as shown yield quantitative composition depth profiles, determine layer thickness, demonstrate interdiffusion and segregation effects even at very low concentrations as well as give structural information such as Si disorder. At the same time, the characterisation of e.g. the final sample set illustrates the necessity of the application of complementary techniques, certainly for the analysis of more complex nanolayer systems. The ability to detect and quantify the atomic redistribution effects that occur during the growth and processing of complex multi-layers makes MEIS a valuable tool in the development of the nanostructures that, as device dimensions are reduced, will become increasingly important.

AUTHOR INFORMATION

Corresponding author

* Email: j.vandenberg@hud.ac.uk

ACKNOWLEDGEMENTS

The support by the European Commmission Research Infrastructure Action under the FP6 "Structuring the European Research Area" Programme through the Integrated Infrastructure Initiative ANNA (contract no. 026134-RII3) and of the UK EPSRC for the funding of the STFC Daresbury MEIS facility is gratefully acknowledged, as is the support of the University of Huddersfield (UK) for the re-establishment of the MEIS facility, previously operated at the Daresbury Laboratory.

REFERENCES

1. G. D. Wilk, R. M. Wallace and J. M. Anthony, J. Appl. Phys. 89 (2001) 5241
2. D. Schlom, S. Guha and S. Datta, MRS Bulletin 33, (2008) 1017
3. J. Robertson, J. Vac. Sci. Technol. B 18, (2000) 1785
4. H. S. Chang, C. N. Wang M.-H. Cho, Moon, C. J. Yim and D.-H. Ko. *Appl.* Phys. Lett. 88 (2006) 081903.
5. J.A Kittl et al. Microelectron Eng.86 (2009) 1789-1795
6. M.A Pawlak et al. Appl. Phys. Letts. 98 (2011) 182902
7. N Menou et al. J. Appl. Phys.106 (2009) 094101
8. M. Popovici et al. Microelectron. Eng. 88 (2011) 1517-1520
9. M. Popovici et al. Phys. Stat. Sol. RRL 1 (2011) 19-21
10. M. Menou et al. Tech. Dig – Int Electron Devices Mtg (2008) 929
11. T. Conard, W. Vandervorst, A. Bergmaier and K. Kimura, J. Vac. Sci. Technol. A30, (2012) 031509
12. R. M. Tromp, Medium Energy Ion Scattering in: D Briggs and P Seah, (Eds.) Practical surface analysis, Vol. 2 Ion and Neutral Spectroscopy. 2nd ed. John Wiley Ltd, New York, (1992)
13. J. F. van der Veen, Surf. Sci. Rep., 5, Nos. 5/6 (1985)
14. T. Gustafsson H.C. Lu, B.W. Busch, W.H. Schulte, E. Garfunkel, Nucl. Instr. Meth. B 183 (2001) 146
15. J.A. van den Berg, D.G. Armour, G. Carter, M. Werner, E.H.J. Collart, R.D. Goldberg, P. Bailey and T.C.Q. Noakes, Appl. Phys. Lett. 85 (2004)3074
16. P. Bailey, T. C. Q. Noakes and P. Woodruff, Surface Sci 426, (1999) 358
17. J. A. van den Berg, S. Zhang, S. Whelan, D. G. Armour, R. D. Goldberg, E. J. H. Collart, P. Bailey, and T. C. Q. Noakes, Nucl. Instrum. Methods Phys. Res. B 183, (2001) 154
18. J. F. Ziegler, J. P. Biersack and U. Littmark, The Stopping and Range of Ions in Solids. New York: Pergamon Press (1985)
19. J. F. Ziegler, SRIM The Stopping and Range of Ions in Matter. http://www.srim.org/
20. M. A. Reading, J. A. van den Berg, P. C. Zalm, D. G. Armour, P. Bailey, T. C. Q. Noakes, A. Parisini, T. Conard, and S. De Gendt, J. Vac. Sci. Technol. B 28, (2010) C1C65
21. W. K. Chu, J. W. Mayer, M. Nicolet, Backscattering Spectrometry (Academic, New York, 1978)
22. H.H. Andersen, F. Besenbacher, P. Loftager, W. Moeller, Phys. Rev. A 21, 1891 (1980)
23. P. Bailey, private communication.
24. J. Kim, W. N. Lennard, C. P. McNorgan, J. Hendriks, I. V. Mitchell, D. Landheer, J. Gredley, Curr. Appl. Phys. 3, 75 (2003)
25. Y. Kido, T. Nishimura, Y.Hoshino, E. Toyoda, T. Nakada, Phys. Rev B 64, 193403
26. K. B. Chung, C.N. Whang, H.S. Chang, D.W. Moon and M.-H. Cho, J. Vac. Sci. Technol. A 25(1), 2007
27. H. Kitano, S.Abo, M. Mizutani, J Tsuchimoto, T Lohner, J. Gyulai,F. Wakaya, M Takai, Nucl. Instr. Meth B 249, 246 (2006)
28. S. Bernardini, M. MacKenzie, O. Buiu, P. Bailey, T.C.Q. Noakes, W.M. Davey, B. Hamilton, S. Hall, Thin Solid Films 517, 459 (2008)

29. L. Miotti, R.P. Pezzi, M. Copel, I.J.R. Baumvol, Nucl. Instrum. Meth B 266, 1162 (2008)
30. IGOR Pro, Wavemetrics (http://www.wavemetrics.com)
31. P. Bailey et al. to be published.
32. F. De Smedt, C. Vinckier, I. Cornelissen, S. De Gendt, M. Heyns, J. Electrochem. Soc. 147 (2000) 1124.
33. J. Swerts et al. *ECS Trans*. 41 (2011) 41.
34. M Popovici et al, ECS Journal of Solid State Science and Technology, **2** (1) N23-N27 (2013).
35. J. A. van den Berg et al., ECS Transact 25(3), (2009) 349-61
36. L. Sygellou, S. Ladas, M. A. Reading, J. A. van den Berg, T. Conard, S De Gendt, Surf. Interface Anal.42 (2010) 1057-1060
37. T. Conard, A. Franquet, W. Vandervorst, M. Reading, J.A. Van den Berg; S. Van Elschocht; T. Schram, S. Degendt, ECS Transactions 16, 433-442, (2008)
38. C. Adelmann, unpublished results
39. L. Sygellou, H. Tielens, C. Adelmann, S. Ladas, Microelect. Eng. 90 (2012) 138-140
40. K. Fröhlich, M. Tˇapajna, A. Rosová, E. Dobrocˇka, K. Hušeková, J. Aarik, A. Aidla, Electrochem. Solid State Lett. 11 (2008) G19–G21.
41. S.K. Kim, S.W. Lee, J.H. Han, B. Lee, S. Han, C.S. Hwang, Adv. Funct. Mater. 20 (2010) 2989–3003.

Figure captions

Figure 1. (a) Energy spectra and model simulations and (b) derived depth profiles for layers D05 (Si/SiO_2/HfO_2) and D06 (Si/SiO_2/HfO_2/DPN) including the nominal layer structure

Figure 2. (a) Energy spectra and model simulations and (b) derived depth profiles for layers D07 (Si/SiO_2/$HfSiO_x$ (60%Hf)) and D08 (Si/SiO_2/$HfSiO_x$ (60%Hf)/DPN) including the nominal layer structure.

Figure 3. (a) MEIS energy spectra (b) and derived depth profiles of a nominal TiN(3nm)/ Al_2O_3(0.9nm)/ HfO_2(2nm)/SiO_2(1nm)/Si metal gate high-k layer stack (schematically shown), showing Hf and Al interdiffusion, upon annealing.

Figure 4. (a) MEIS energy spectra and model simulations and (b) simulated depth profiles for sample D02 (Si/TiN) including the nominal layer structure.

Figure 5. (a) MEIS energy spectra and model simulations and (b) simulated depth profiles for samples D05 (Si/TiN/Sr-rich STO) and D06 (Si/TiN/Sr-rich STO 15s 650°C), including the nominal layer structure.

Figure 6. (a) MEIS energy spectra and model simulations and (b) simulated depth profiles for samples D11 (Si/TiN/stoich STO/TiN) and D12 (Si/TiN/stoich STO/TiN, 650°C 15s) shown schematically.

Figure 7. (a) MEIS energy spectra and model simulations and (b) simulated depth profiles for the (Si/TiN/Ru/TiO_2) layer structure, shown schematically. The interlayer containing Ti, O and Ru is indicated.

Figure 8. Energy spectrum and model simulations of a (Si/TiN/Ru/TiO_2 -1%Al, 370°C, 60 s) layer structure. The Al peak occurs at around 148 keV as shown in the inset. Al is seen to have segregated towards the top of the layer after annealing.